photonics

Communication

Modification of the Emission Spectrum of a Quantum Emitter in the Vicinity of Bismuth Chalcogenide Microparticles

Margarita-Georgia Papadaki [1], Nikolaos Kyvelos [1,2], Emmanuel Paspalakis [3] and Vassilios Yannopapas [1,*]

1 Department of Physics, School of Applied Mathematical and Physical Sciences, National Technical University of Athens, GR157 80 Athens, Greece; margi98@windowslive.com (M.-G.P.); nikoskyvelos@mail.ntua.gr (N.K.)
2 POLIMA—Center for Polariton-Driven Light–Matter Interactions, University of Southern Denmark, Campusvej 55, DK5230 Odense, Denmark
3 Department of Materials Science, University of Patras, GR265 04 Patras, Greece; paspalak@upatras.gr
* Correspondence: vyannop@mail.ntua.gr

Abstract: We examine theoretically the effect of bismuth chalcogenide microparticles on the spontaneous emission of a double-V-type quantum emitter in free space. We have found, in particular, that the presence of a single microparticle causes a high degree of quantum interference in the way the quantum emitter releases energy in the process of spontaneous emission. This, in turn, leads to significant changes in the spectrum of the emitted energy. The quantum emitter's initial state is crucial to how the energy is released in the presence of the microparticle. This observation has potential implications for quantum computing, particularly for reading the state of atomic qubits. When two microparticles are present, the effect is more pronounced, particularly when the quantum emitter is located in the gap between the particles.

Keywords: quantum interference; spontaneous emission; polar materials

check for updates

Citation: Papadaki, M.-G.; Kyvelos, N.; Paspalakis, E.; Yannopapas, V. Modification of the Emission Spectrum of a Quantum Emitter in the Vicinity of Bismuth Chalcogenide Microparticles. *Photonics* **2023**, *10*, 658. https://doi.org/10.3390/photonics10060658

Received: 19 April 2023
Revised: 12 May 2023
Accepted: 24 May 2023
Published: 7 June 2023

1. Introduction

Quantum plasmonics is a rapidly growing field that combines quantum mechanics and plasmonics, the study of the collective oscillations of electrons in metals or metal-like structures [1–4]. In quantum plasmonics, the principles of quantum mechanics are used to manipulate and control light at the nanoscale. This opens up new avenues for applications in photonics and sensing, such as ultra-small optical devices, high-resolution imaging, and biosensing [5]. One of the key features of quantum plasmonics is the use of quantum entanglement, where the quantum states of two or more particles are correlated in such a way that the state of one particle affects the state of another. This provides new opportunities for applications in quantum communication, cryptography, and quantum computing. Overall, quantum plasmonics and quantum nanophotonics represent a promising direction for future technological advancements in the fields of nanophotonics and quantum technologies [6].

The implementation of quantum technologies that utilize plasmonic devices requires a significant interaction between a quantum emitter (QE) and light. This connection can be reinforced through the integration of the emitter with a plasmonic structure that intensifies the emission rates by elevating the availability of the local density of states (LDOS) to the emitter. The above phenomenon is known in the literature as the Purcell effect [7] and has since been acknowledged as a crucial aspect of quantum plasmonics. The so-called Purcell factor measures the change in the spontaneous emission (SE) rate of the emitter in the presence of a photonic/plasmonic environment in comparison to its rate in vacuum [8,9].

The mainstream materials supporting plasmon excitations are noble metals: silver, gold, and copper. However, due to their intrinsic losses, mainly in the optical regime, alternative materials have been suggested in order to mitigate losses. Such materials are high-index dielectrics and semiconductors, such as Si, GaAs, and AlGaAs [10]. The use of high-refractive-index materials in plasmonics offers several benefits, such as improved light–matter interactions, decreased losses, and increased compatibility with silicon-based electronics [11]. These benefits make plasmonics with high-refractive-index materials a rapidly growing field for applications in areas such as sensing, photonics, and quantum computing [12].

A recent advancement in materials science has given rise to chalcogenides, which showcase impressive dielectric properties due to their robust phonon resonances in the THz range. They are materials that contain elements from the chalcogen group on the periodic table, including sulfur (S), selenium (Se), and tellurium (Te). These materials have unique optical and electronic properties and have been of great interest for photonics and optoelectronics [13–15]. Bismuth chalcogenides are known for their high refractive index [16] and strong light confinement properties, making them attractive for use in nanophotonics and other optical technologies [17,18]. In recent years, chalcogenides have been particularly well studied for their potential use in polaritonic excitations and for enhancing light–matter interactions in quantum technologies [19].

The polaritonic excitations result in the strong confinement of light and high field enhancement at their surfaces. On the other hand, noble metal nanostructures may exhibit enhanced Purcell factors due to plasmon resonances; however, their large ohmic losses hinder efficient coupling with quantum emitters (QEs) [20]. Bismuth chalcogenides, on the other hand, exhibit lower ohmic losses in combination with high field enhancement, leading to improved coupling with QEs through polaritonic excitations [21–23]. The polaritonic excitations in these materials are eigenstates of the electromagnetic field and result in a high partially local density of states (PLDOS) around the bismuth chalcogenides particles [24], thus leading to substantial modifications and control over the spontaneous emission rate of a nearby QE.

In the present work, we will study the effect of the presence of bismuth chalcogenide microparticles on the spontaneous emission spectrum of a multi-level QE. Namely, we show that when the QE is placed near a single bismuth chalcogenide microparticle or in between two such particles, the spontaneous emission of the QE depends strongly on the initial state of the QE. This occurs as the presence of the microparticles boosts the phenomenon of quantum interference of spontaneous emission paths, which, in turn, generates the dependence of the emission spectrum on the initial quantum state of the QE.

2. Quantum Interference in a Double-V-Type Quantum Emitter

Quantum interference (QI) is a result of the simultaneous emission of two nearby excited states of a quantum emitter into a shared ground state, creating the possibility for interference between the two emission paths. The typical quantum system for this to happen is the V-type system. The spectral pattern of the emission is shaped by the energy structure and quantum coherence; however, for interference to happen, the transition dipole moments of the two emission pathways in the V-type system must not be perpendicular. Achieving this in a pure quantum system can be challenging. However, Agarwal demonstrated in 2000 [25] that the creation of an anisotropic quantum vacuum can result in QI between the decay channels of perpendicular nearby states [26]. This occurs when there is a substantial difference in decay rates between orthogonal dipole moments, resulting in a noticeable degree of QI [27]. This phenomenon in a quantum emitter could result in exciting phenomena in quantum optics and coherent nonlinear optics, including coherent population trapping [28–32], a large degree of entanglement [33–35], amplification without inversion [36,37], controllable spontaneous emission or resonance fluorescence spectra [26,38–40], optical transparency accompanied with slow light [41–43], strengthened Kerr nonlinearity [44–48], and distinct non-Markovian dynamics [49].

Figure 1 shows the quantum system we study in the present work. We consider a double-V-type quantum system as having two closely lying upper states, $|2\rangle$ and $|3\rangle$, and two lower-energy states, $|0\rangle$ and $|1\rangle$. We take states $|2\rangle$ and $|3\rangle$ to characterize two Zeeman sublevels. Then, the dipole moment operator is taken as $\vec{\mu} = \mu'(|2\rangle\langle 0|\hat{\varepsilon}_- + |3\rangle\langle 0|\hat{\varepsilon}_+) +$

$\mu(|2\rangle\langle 1|\hat{\varepsilon}_- + |3\rangle\langle 1|\hat{\varepsilon}_+) + \text{H.c.}$, where $\hat{\varepsilon}_\pm = (\mathbf{e}_z \pm i\mathbf{e}_x)/\sqrt{2}$, is used for the description of right-rotating ($\hat{\varepsilon}_+$) or left-rotating ($\hat{\varepsilon}_-$) unit vectors. Furthermore, the dipole matrix elements μ, μ' are taken to be real.

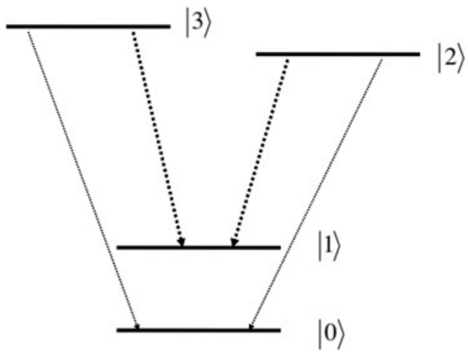

Figure 1. The quantum system under consideration is a double-V-type system. Two upper states $|2\rangle$ and $|3\rangle$ decay spontaneously to the two lower states $|0\rangle$ and $|1\rangle$.

Spontaneous emission occurs from states $|2\rangle$ and $|3\rangle$ to the lower state $|0\rangle$ with decay rates $2\gamma_2'$ and $2\gamma_3'$, respectively. Furthermore, spontaneous decay occurs from states $|2\rangle$ and $|3\rangle$ to the lower state $|1\rangle$ with decay rates $2\gamma_2$ and $2\gamma_3$, respectively. We assume that the transitions $|2\rangle$ and $|3\rangle$ to $|1\rangle$ are in energies that are influenced by the presence of nearby macroscopic objects (bismuth chalcogenide microparticles in our case). The transitions $|2\rangle$ and $|3\rangle$ to $|0\rangle$ are in quite different energies from the transitions $|2\rangle$ and $|3\rangle$ to $|1\rangle$, and we assume that they are not influenced by the presence of the microparticles. So, these transitions occur from the interaction of the quantum system with free-space vacuum, and we will address this decay below as the free-space decay. In the following part of the paper, we will calculate the spontaneous decay rate of this process.

The method of calculation of the spontaneous emission spectrum is based on the probability amplitude approach [50]. Under the application of the rotating-wave approximation and using the Weisskopf–Wigner theory of spontaneous emission, the probability amplitudes of states $|2\rangle$, $|3\rangle$, and $|0\rangle$ are given by [26,42,51] (we assume $\hbar = 1$ throughout this work):

$$\dot{b}_2(t) = \frac{1}{2}(i\omega_{32} - 2\gamma_2 - 2\gamma_2')b_2(t) - \kappa_3 b_3(t)\,, \quad (1)$$

$$\dot{b}_3(t) = -\kappa_2 b_2(t) - \frac{1}{2}(i\omega_{32} + 2\gamma_3 + 2\gamma_3')b_3(t)\,, \quad (2)$$

$$\dot{b}_{\mathbf{k}}(t) = -i\delta_{\mathbf{k}} b_{\mathbf{k}}(t) - i g_{\mathbf{k}2} b_2(t) - i g_{\mathbf{k}3} b_3(t)\,, \quad (3)$$

here $\omega_{32} = \omega_3 - \omega_2$, where ω_n is the angular frequency of level n (with $n = 2, 3$). Furthermore, the coupling constant of transition $|n\rangle \leftrightarrow |0\rangle$ with the $\mathbf{k}$-th vacuum mode is $g_{\mathbf{k}n} = -i\sqrt{\frac{2\pi\omega_{\mathbf{k}}}{V}}\vec{\mu}'_{n0} \cdot \hat{\varepsilon}_{\mathbf{k}}$. In addition, $\hat{\varepsilon}_{\mathbf{k}}$ denotes the unit polarization vector of the $\mathbf{k}$-th vacuum mode with angular frequency $\omega_{\mathbf{k}}$, and V is the quantization volume. Furthermore, $\delta_{\mathbf{k}} = \omega_{\mathbf{k}} - (\omega_{20} + \omega_{30})/2$, where $\omega_{n0} = \omega_n - \omega_0$. Finally, important quantities are the parameters κ_2 and κ_3, which describe the coupling coefficients between states $|2\rangle$ and $|3\rangle$ due to spontaneous emission in the altered photonic environment due to the presence of the microparticles [25,51–56]. We will call these terms below the QI terms. The values of γ_2 and γ_3, and κ_2 and κ_3, are given by [51,53]

$$\gamma_2 = \frac{1}{2}\left(\Gamma_{\perp}^{\omega_{21}} + \Gamma_{\parallel}^{\omega_{21}}\right), \tag{4}$$

$$\gamma_3 = \frac{1}{2}\left(\Gamma_{\perp}^{\omega_{31}} + \Gamma_{\parallel}^{\omega_{31}}\right), \tag{5}$$

$$\kappa_2 = \frac{1}{2}\left(\Gamma_{\perp}^{\omega_{21}} - \Gamma_{\parallel}^{\omega_{21}}\right), \tag{6}$$

$$\kappa_3 = \frac{1}{2}\left(\Gamma_{\perp}^{\omega_{31}} - \Gamma_{\parallel}^{\omega_{31}}\right). \tag{7}$$

In the above equations, $\mathbf{r}$ refers to the position of the quantum emitter and $\omega_{n1} = \omega_n - \omega_1$. Furthermore, it is convenient to define the spontaneous emission rates normal and parallel to the surface of the microstructure of interest, as $\Gamma_{\perp}^{\omega_{n1}} = \mu^2\omega_{n1}^2 \text{Im}[G_{\perp}(\mathbf{r},\mathbf{r};\omega_{n1})]$ and $\Gamma_{\parallel}^{\omega_{n1}} = \mu^2\omega_{n1}^2 \text{Im}[G_{\parallel}(\mathbf{r},\mathbf{r};\omega_{n1})]$, respectively.

When the two upper levels $|2\rangle$ and $|3\rangle$ are degenerate, then $\omega_{21} = \omega_{31} = \bar{\omega}$ $(\omega_{32} = 0)$. Then, $\gamma_2 = \gamma_3 = \bar{\gamma} = (\Gamma_{\perp} + \Gamma_{\parallel})/2$ and $\kappa_2 = \kappa_3 = \bar{\kappa} = (\Gamma_{\perp} - \Gamma_{\parallel})/2$. We can now define the spontaneous decay rates $\Gamma_{\perp,\parallel} = \mu^2\bar{\omega}^2 \text{Im}[G_{\perp,\parallel}(\mathbf{r},\mathbf{r};\bar{\omega})]$, and the degree of QI is given by

$$p = \frac{\bar{\kappa}}{\bar{\gamma}} = \frac{\Gamma_{\perp} - \Gamma_{\parallel}}{\Gamma_{\perp} + \Gamma_{\parallel}}. \tag{8}$$

In the case that $p = 1$, we have maximum QI. This can be achieved by placing the emitter close to a structure that completely inhibits $\Gamma_{\parallel}$. Obviously, when the emitter is placed in vacuum, $\Gamma_{\perp} = \Gamma_{\parallel}$ and $\bar{\kappa} = 0$, so no QI occurs in the system, as should be expected.

The spontaneous emission spectrum in the long-time limit is given by [50]

$$S(\delta_{\mathbf{k}}) \propto |b_{\mathbf{k}}(t \to \infty)|^2. \tag{9}$$

In order to calculate the spectrum, we apply the Laplace transform in Equations (1)–(3), and use the final value theorem [50] to obtain [42]

$$\begin{aligned} S(\delta_{\mathbf{k}}) \propto\; & \gamma_2' \frac{\left|(-i\delta_{\mathbf{k}} + i\omega_{32}/2 + \gamma_3 + \gamma_3')b_2(0) - \kappa_3 b_3(0)\right|^2}{|D(\delta_{\mathbf{k}})|^2} \\ + \; & \gamma_3' \frac{\left|(-i\delta_{\mathbf{k}} - i\omega_{32}/2 + \gamma_2 + \gamma_2')b_3(0) - \kappa_2 b_2(0)\right|^2}{|D(\delta_{\mathbf{k}})|^2}, \end{aligned} \tag{10}$$

where

$$\begin{aligned} D(\delta_{\mathbf{k}}) =\; & (-i\delta_{\mathbf{k}} + i\omega_{32}/2 + \gamma_3 + \gamma_3')(-i\delta_{\mathbf{k}} - i\omega_{32}/2 \\ + \; & \gamma_2 + \gamma_2') - \kappa_2\kappa_3. \end{aligned} \tag{11}$$

3. Results and Discussion

The computational setup of the present work is shown in Figure 2. However, we first assume that the QE of Figure 1 is in vacuum. The corresponding spontaneous emission spectrum is presented in Figure 3. It is calculated using Equation (10) and presuming that the emitter is in a vacuum environment. The results show that when $\gamma_2' = \gamma_3' = \gamma_2 = \gamma_3 = \gamma$, and $\omega_{32} = 0$, the spectrum is a Lorentzian with the following form:

$$S(\delta_{\mathbf{k}}) \propto \frac{\gamma}{\delta_{\mathbf{k}}^2 + 4\gamma^2}. \tag{12}$$

This means that the shape of the spectrum is independent of the specific initial conditions. However, when $\omega_{32} \neq 0$, the spectrum is given by the sum of two Lorenzians located at $\pm\omega_{32}/2$ and weighted by $|b_2(0)|^2$ and $|b_3(0)|^2$, respectively. The spectrum can be strongly influenced by the initial conditions in this case, as $|b_2(0)|^2 \neq |b_3(0)|^2$ and therefore the two Lorenzians will have different heights. However, for the particular parameters chosen in Figure 3b, the initial conditions have no impact on the shape of the spectrum, since $|b_2(0)|^2 = |b_3(0)|^2 = 1/2$.

Figure 2. Computational setup: (**a**) the 4-level QE of Figure 1 is placed next to a single Bi_2Te_3 microsphere of radius 2 μm and (**b**) in the middle of a dimer of 2 μm Bi_2Te_3 microspheres.

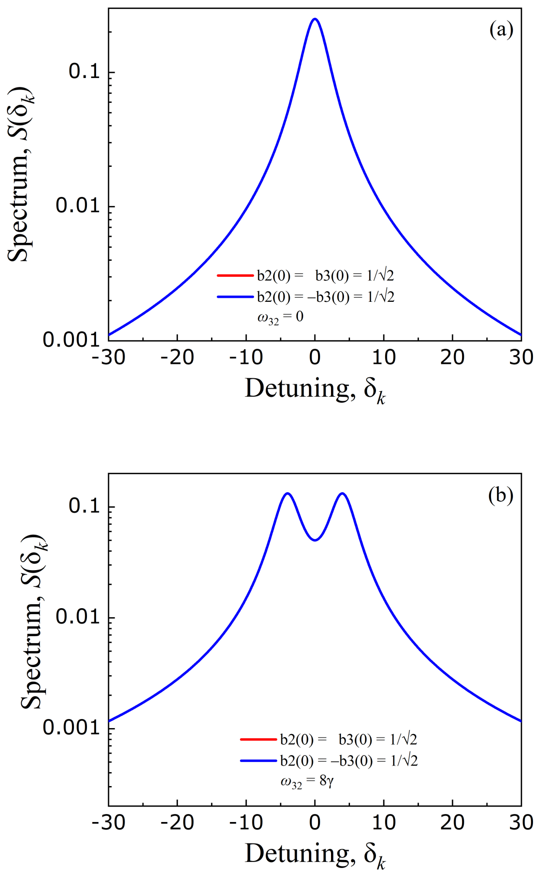

Figure 3. The spontaneous emission spectrum $S(\delta_{\mathbf{k}})$ (in arbitrary units) of a quantum system in a vacuum state is described by Equation (10). The plot in (**a**) shows the case when $\omega_{32} = 0$, while plot (**b**) shows the case when $\omega_{32} = 8\gamma$. The blue lines in both plots correspond to $b_2(0) = b_3(0) = \frac{1}{\sqrt{2}}$, and the red lines correspond to $b_2(0) = \frac{1}{\sqrt{2}}$, $b_3(0) = -\frac{1}{\sqrt{2}}$. The parameters used in the plot are $\gamma'2 = \gamma'3 = \gamma_2 = \gamma_3 = \gamma$, and $\delta_{\mathbf{k}}$ is measured in units of γ. In the vacuum, $\kappa_2 = \kappa_3 = 0$. Since the QE lies in vacuum, both blue and red lines are identical due to the absence of QI.

Next, we assume that the QE of Figure 1 is placed in the vicinity of a single Bi_2Te_3 microsphere with a 2 μm radius (see Figure 2a). The dielectric function of Bi_2Te_3 is provided by a triple sum of Lorentz-oscillator-type terms [18]

$$\epsilon(\omega) = \sum_{j=\alpha,\beta,f} \frac{\omega_{pj}^2}{\omega_{0j}^2 - \omega^2 - i\gamma_j\omega}. \tag{13}$$

The subscripts in Equation (13) represent contributions from α and β phonons, as well as bulk free-charge carriers f. These parameters can be found in [18] and are derived from fitting to experimental data on bulk Bi_2Te_3 found in [57]. Bi_2Te_3 is a well-known topological insulator, and its dielectric function has an extra component due to surface states, which decrease as the sphere radius increases [17]. This surface-state term only has a substantial impact on nanospheres, and is negligible in our case as we are using microspheres. We note that the dielectric function of Equation (13) assumes colossal values in the THz regime due to the existence of phonon–polariton modes [17].

In order to calculate the parameters of Equations (7) and (8), we need the spontaneous emission rates for a radially and tangentially (relative to a sphere) oriented dipole (QE) for the case of a single Bi_2Te_3 microsphere. These are calculated via the EM Green's tensor [58,59] based on Mie scattering theory. Figure 4 shows the degree of QI, p Equation (8), as a function of frequency and distance from the surface of a single Bi_2Te_3 microsphere [22]. It is evident that there is a wide region of both parameters (frequency and distance), where the degree of QI assumes very high values. This region spans roughly, in frequency range, from 10 to 14 THz and, in distance range, from 0.8 to 1.7 μm. We note that, when conducting high-precision quantum-optics experiments to investigate QI-related phenomena, using the photonic reservoir of modes supported by a Bi_2Te_3 sphere is a more reliable method. This is because the QI values are much higher across a broad range of frequencies and distances from the surface, and a precise positioning of the QE is not critical. Similar effects have also been reported for another type of bismuth chalcogenide microparticle, namely, Bi_2Se_3 microparticles [23], whose dielectric function is similar to that of Equation (13). We want to emphasize that for bismuth chalcogenide spheres with smaller sizes, i.e., nanospheres, the degree of interference is reduced, and a significant enhancement of the Purcell factors is obtained; therefore, the observed phenomena reported in our manuscript cannot be seen.

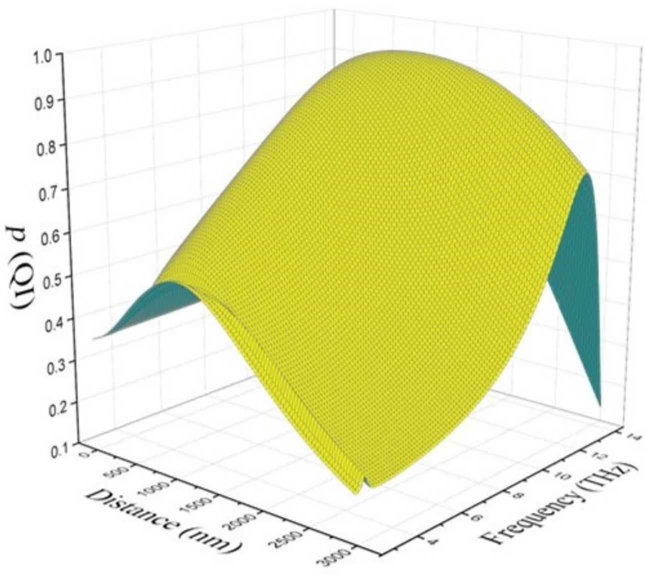

Figure 4. Degree of QI, p, as a function of both frequency and distance D from a 2 μm Bi_2Te_3 microsphere.

Based on Figure 4, the highest value of p (QI) for a 2 μm Bi_2Te_3 microsphere is $p = 0.95$ and occurs at frequency 12.1 THz, when a QE (dipole) is placed at 2 μm from the surface of the microsphere. In this case, the corresponding spontaneous emission rates are $\gamma_\perp = 16.34\gamma$ (radially oriented dipole) and $\gamma_\parallel = 0.41\gamma$ (tangentially oriented dipole). This remarkable difference in the spontaneous emission rates between the two different dipole orientations is the source of the high value $p = 0.95$ of the degree of QI. By substituting the above values of $\gamma_\perp$ and $\gamma_\parallel$ into Equations (7), we obtain the corresponding values for $\gamma_2, \gamma_3, \kappa_2, \kappa_3$ needed for the calculation of the spectrum of Equation (10). The results are depicted in Figure 5. Namely, in Figure 5, we depict the free-space spontaneous emission spectrum Equation (10) for the same parameters as in Figure 3, except from the fact that the QE of Figure 6 is not assumed to be in free space but close to a Bi_2Te_3 microsphere. We observe that the degeneracy of the spectrum for the two different initial states of the QE no longer exists. Even more, the presence of the Bi_2Te_3 microparticle has opposite effects on the emission spectrum for the two initial quantum states. Roughly speaking, for the anti-symmetric state ($b_2(0) = \frac{1}{\sqrt{2}}$, $b_3(0) = -\frac{1}{\sqrt{2}}$) there is a 20-fold increase in the peak value, whereas for the symmetric state ($b_2(0) = b_3(0) = \frac{1}{\sqrt{2}}$) there is a 10-fold decrease in the same quantity. This is a strong manifestation of the symmetry break introduced by the presence of the microsphere, which creates an artificial 'anisotropic vacuum' [25], which, in turn, promotes the presence of QI in the spontaneous emission paths of the QE of Figure 1. At the same time, we observe that the double-peak structure, in the absence of the microparticle and for $\omega_{32} = 8\gamma$ (see Figure 3), becomes single-peaked when it is present. This is due to the higher values of the rates $\kappa_{2,3}, \gamma_{2,3}$, making the two Lorentzian peaks of the vacuum case merge into a single peak [42] when the bismuth chalcogenide microparticle is present. Contrary to the case of $\omega_{32} = 0$, when $\omega_{32} \neq 0$, there are no simple formulae for the emission spectrum $S(\delta_{\mathbf{k}})$, such as those of Equations (14) and (15).

The observed behavior of Figure 5a ($\omega_{32} = 0$) can be explained by looking at Equation (10) and considering different initial conditions. When $b_2(0) = b_3(0) = 1/\sqrt{2}$, the resulting spectrum takes the form

$$S(\delta_{\mathbf{k}}) \propto \frac{\gamma}{\delta_{\mathbf{k}}^2 + (\gamma + \gamma_\perp)^2}. \tag{14}$$

In this case, $\gamma_\perp$ is significantly higher than the decay rate in vacuum, which results in a significant increase in the denominator of the spectrum, leading to an overall suppression of the spectrum. On the other hand, when $b_2(0) = 1/\sqrt{2}$ and $b_3(0) = -1/\sqrt{2}$, the spectrum takes the form

$$S(\delta_{\mathbf{k}}) \propto \frac{\gamma}{\delta_{\mathbf{k}}^2 + (\gamma + \gamma_\parallel)^2}. \tag{15}$$

In this case, $\gamma_\parallel$ is significantly lower than the corresponding vacuum value, which leads to an enhancement of the spectrum and a narrowing of the line.

Next, we consider the case of a dimer of Bi_2Te_3 microspheres with a 2 μm radius, where the QE of Figure 1 is placed between the microspheres at equal distance from each sphere (see Figure 2b). With this particular setup, the degree of QI, p, is boosted even further due to the strong confinement of the photonic modes in the gap between the microspheres [23]. Figure 6 shows the spontaneous emission rates for the radial (a) and tangential (b) orientation of the QE relative to the sphere surfaces for three different sphere separations (gaps): $D = 2000, 200, 100$ nm. First of all, it is evident that, overall, the spontaneous emission rates significantly increase with decreasing gap size for both types of QE orientations. This is due to the enhancement of the PLDOS within the gap, which acts as a cavity resonator. Secondly, the increase is not the same for both orientations, leading to very high values for the degree of QI, p. Evidently, from Figure 6c, we can see that p reaches values very close to unity. As an example, for a gap size of 2 μm and frequency of 11.6 THz, the spontaneous emission rates become $\gamma_\perp = 69.67\gamma$ (radially oriented dipole) and $\gamma_\parallel = 0.35\gamma$ (radially oriented dipole), which provide a value of $p = 0.99$ for the degree of QI. By substituting the above values of $\gamma_\perp$ and $\gamma_\parallel$ into Equations (7), we obtain the corresponding values for $\gamma_2, \gamma_3, \kappa_2, \kappa_3$ needed for the calculation of the spectrum of Equation (10). The results are depicted in Figure 7. It is evident that the findings of Figure 5 are even more pronounced for the case of the microsphere dimer of Figure 7. Especially for $\omega_{32} = 0$, the spectrum for the symmetric case (top panel of Figure 7) is almost flattened out. We note that the spectral differences in Figure 7 can, again, be explained in terms of Equations (14) and (15). It is worth noting that more complicated setups involving additional microspheres are not required, given that the dimer already produces a value of $p = 0.99$, which is almost as high as the theoretical maximum of unity.

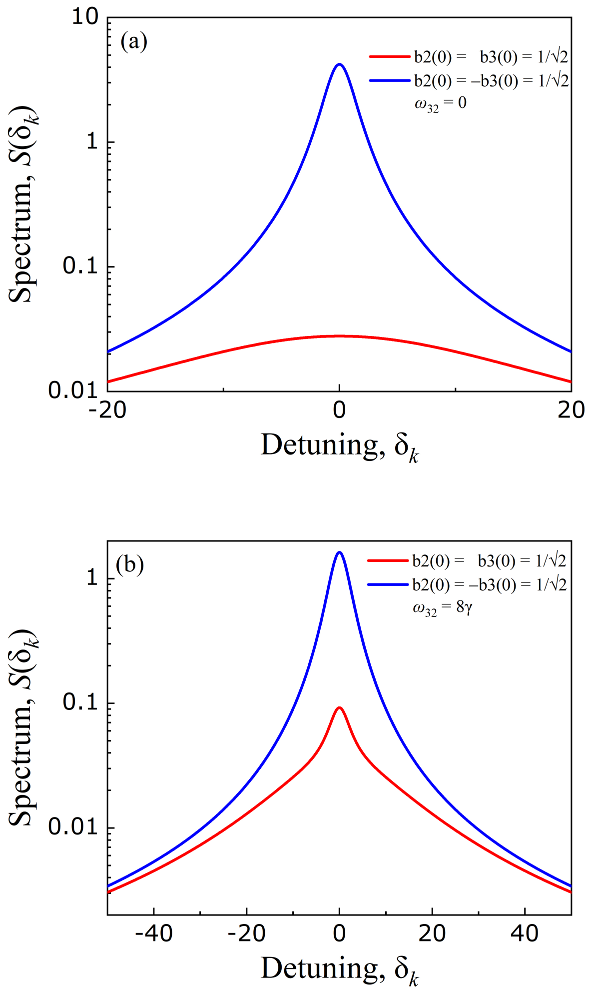

Figure 5. The spontaneous emission spectrum $S(\delta_{\mathbf{k}})$ (in arbitrary units) of a quantum system placed near a single 2 μm Bi_2Te_3 sphere (see Figure 2a). The plot in (**a**) shows the case when $\omega_{32} = 0$, while plot (**b**) shows the case when $\omega_{32} = 8\gamma$. The solid lines in both plots correspond to $b_2(0) = b_3(0) = \frac{1}{\sqrt{2}}$, and the dashed lines correspond to $b_2(0) = \frac{1}{\sqrt{2}}$, $b_3(0) = -\frac{1}{\sqrt{2}}$. The parameters used in the plot are $\gamma_2' = \gamma_3' = \gamma$, and $\delta_{\mathbf{k}}$ is measured in units of $\gamma_2, \gamma_3, \kappa_2, \kappa_3$, which are influenced by the presence of the 2 μm Bi_2Te_3 microsphere and are calculated for a frequency of 12.1 THz at a distance $D = 1$ μm from the microsphere: $\gamma_2 = \gamma_3 = 8.38\gamma$ and $\kappa_2, \kappa_3 = 7.97\gamma$. The corresponding degree of QI is $p = 0.95$.

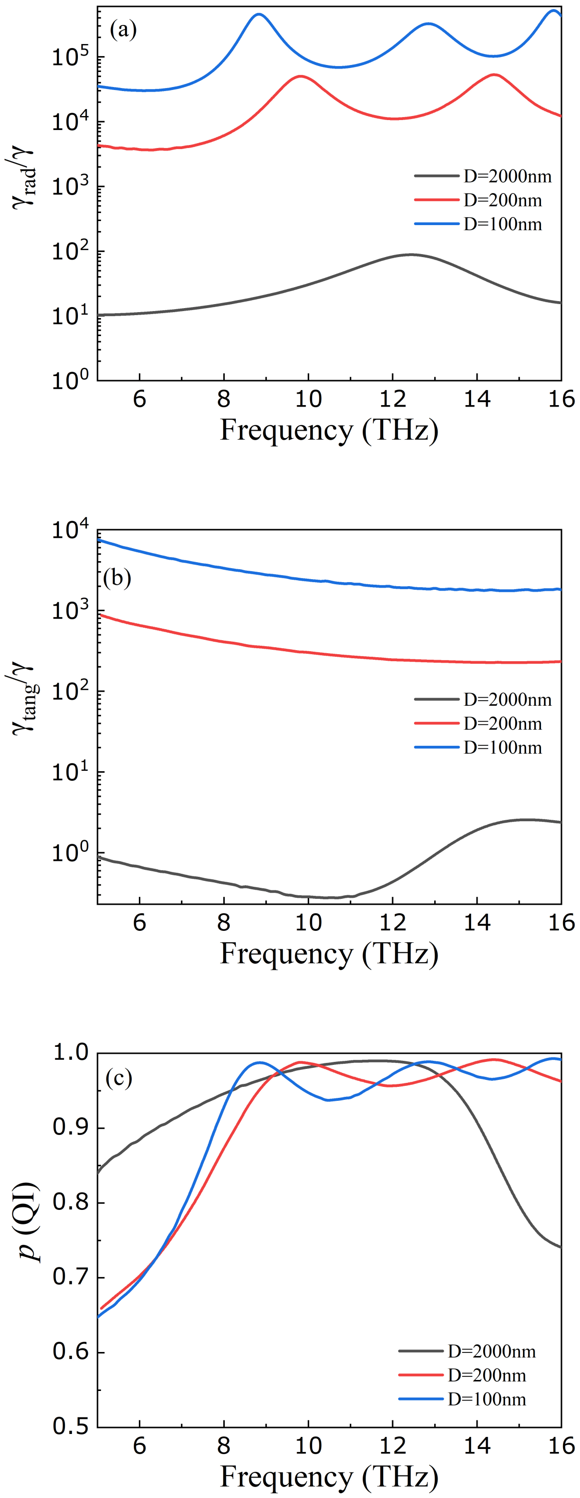

Figure 6. Spectra of SE rates for a dipole that is normally (**a**) and tangentially (**b**) oriented with respect to the surfaces of a dimer of Bi_2Te_3 microspheres with 2 μm radius and for different gap sizes D: $D = 2000$ nm, $D = 200$ nm, $D = 100$ nm. In (**c**), we show the corresponding QI factor for the SE rates given in (**a**,**b**).

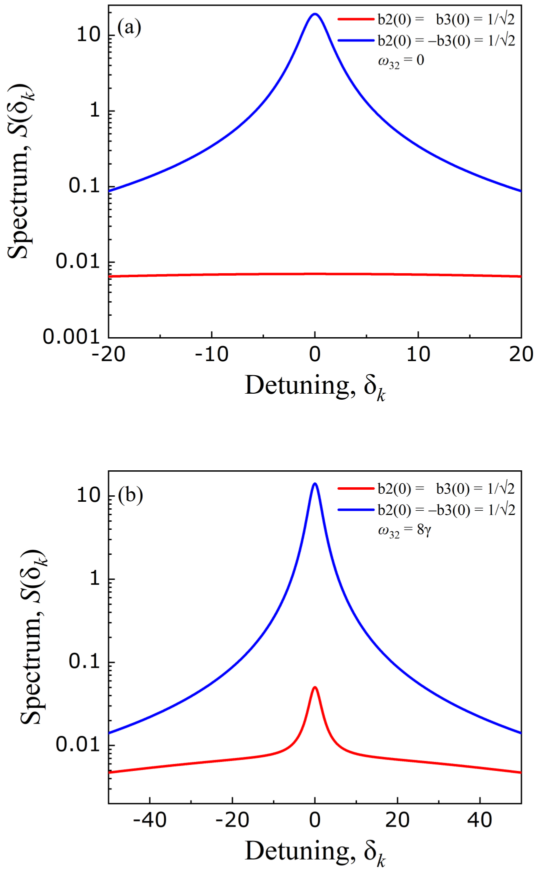

Figure 7. The spontaneous emission spectrum $S(\delta_{\mathbf{k}})$ (in arbitrary units) of a quantum system between two 2 μm Bi_2Te_3 spheres in the middle of the gap between them (see Figure 2b). The plot in (**a**) shows the case when $\omega_{32} = 0$, while plot (**b**) shows the case when $\omega_{32} = 8\gamma$. The solid lines in both plots correspond to $b_2(0) = b_3(0) = \frac{1}{\sqrt{2}}$, and the dashed lines correspond to $b_2(0) = \frac{1}{\sqrt{2}}$, $b_3(0) = -\frac{1}{\sqrt{2}}$. The parameters used in the plot are $\gamma_2' = \gamma_3' = \gamma$, and $\delta_{\mathbf{k}}$ is measured in units of $\gamma_2, \gamma_3, \kappa_2, \kappa_3$, which are influenced by the presence of the dimer of the 2 μm Bi_2Te_3 microspheres and are calculated for a frequency of 11.6 THz for a gap distance $D = 2$ μm between the microspheres: $\gamma_2 = \gamma_3 = 35.01\gamma$ and $\kappa_2, \kappa_3 = 34.66\gamma$. The corresponding degree of QI is $p = 0.99$.

4. Conclusions

We have investigated the impact of bismuth chalcogenide microparticles on the spontaneous emission of a double-V-type quantum emitter in free space. Specifically, we analyzed a system where one V-type transition is influenced by the interaction with the microparticles, while the other V-type transition interacts solely with a free-space vacuum. We demonstrated numerically that the presence of a single bismuth chalcogenide microparticle evokes a high degree of quantum interference in the spontaneous emission paths of the quantum emitter, which, in turn, leads to dramatic modifications to the spontaneous emission spectrum relative to the case where the microparticle is absent. Moreover, in the presence of the bismuth chalcogenide microparticle, the spontaneous emission spectrum depends critically on the initial state of the quantum. This effect would have potential application in quantum computing for reading out the state of atomic qubits. These phenomena are more magnified for the case of a dimer of bismuth chalcogenide microparticles, in which case the quantum emitter resides in the gap space between the microparticles.

Author Contributions: Conceptualization, V.Y.; methodology, M.-G.P., V.Y. and E.P.; software, N.K.; validation, N.K., V.Y., M.-G.P. and E.P.; investigation, M.-G.P., V.Y., N.K. and E.P.; resources, E.P. and V.Y.; data curation, M.-G.P.; writing—original draft preparation, V.Y.; writing—review and editing, N.K., V.Y., M.-G.P. and E.P.; visualization, V.Y.; supervision, V.Y.; project administration, V.Y., E.P.; funding acquisition, N.K. All authors have read and agreed to the published version of the manuscript.

Funding: The Center for Polariton-driven Light–Matter Interactions (POLIMA) is sponsored by the Danish National Research Foundation (Project No. DNRF165).

Institutional Review Board Statement: Not applicable.

Informed Consent Statement: Not applicable.

Data Availability Statement: The data presented in this study are available on resonable request from the corresponding author.

Conflicts of Interest: The authors declare no conflict of interest.

References

1. Tame, M.; McEnery, K.; Özdemir, Ş.; Lee, J.; Maier, S.A.; Kim, M.S. Quantum plasmonics. *Nat. Phys.* **2013**, *9*, 329. [CrossRef]
2. Lodahl, P.; Mahmoodian, S.; Stobbe, S. Interfacing single photons and single quantum dots with photonic nanostructures. *Rev. Mod. Phys.* **2015**, *87*, 347. [CrossRef]
3. Hohenester, U. *Nano and Quantum Optics: An Introduction to Basic Principles and Theory*; Springer: Cham, Switzerland, 2019.
4. Tserkezis, C.; Fernandez-Dominguez, A.I.; Dias Gonçalves, P.A.; Todisco, F.; Cox, J.D.; Busch, K.; Stenger, N.; Bozhevolnyi, S.I.; Mortensen, N.A.; Wolff, C. On the applicability of quantum-optical concepts in strong-coupling nanophotonics. *Rep. Prog. Phys.* **2020**, *83*, 082401. [CrossRef] [PubMed]
5. Schuller, J.; Barnard, E.; Cai, W.; Jun, Y.C.; White, J.S.; Brongersma, M.L. Plasmonics for extreme light concentration and manipulation. *Nat. Mater.* **2010**, *9*, 193. [CrossRef] [PubMed]
6. Baranov, D.G.; Wersäll, M.; Cuadra, J.; Antosiewicz, T.J.; Shegai, T. Novel Nanostructures and Materials for Strong Light–Matter Interactions. *ACS Photonics* **2018**, *5*, 24. [CrossRef]
7. Purcell, E.M. Spontaneous emission probabilities at radio frequencies. *Phys. Rev.* **1946**, *69*, 681.
8. Drexhage, K.H. Influence of a dielectric interface on fluorescence decay time. *J. Luminesc.* **1970**, *1*, 693–701. [CrossRef]
9. Drexhage, K.H. Interaction of light with monomolecular dye lasers. *Prog. Opt.* **1974**, *12*, 163–232.
10. West, P.R.; Ishii, S.; Naik, G.V.; Emani, N.K.; Shalaev, V.M.; Boltasseva A. Searching for better plasmonic materials. *Laser Photon. Rev.* **2010**, *4*, 795. [CrossRef]
11. Naik, G.V.; Shalaev, V.M.; Boltasseva, A. Alternative plasmonic materials: Beyond gold and silver. *Adv. Mater.* **2013**, *25*, 3264. [CrossRef]
12. Kinsey, N.; Ferrera, M.; Shalaev, V.M.; Boltasseva, A. Examining nanophotonics for integrated hybrid systems: A review of plasmonic interconnects and modulators using traditional and alternative materials. *J. Opt. Soc. Am. B Opt. Phys.* **2015**, *32*, 121. [CrossRef]
13. Xia, C.; Li, J. Recent advances in optoelectronic properties and applications of two-dimensional metal chalcogenides. *J. Semicond.* **2016**, *37*, 051001. [CrossRef]
14. You, J.W.; Bongu, S.R.; Bao, Q.; Panoiu, N.C. Nonlinear optical properties and applications of 2D materials: Theoretical and experimental aspects. *Nanophotonics* **2018**, *8*, 63. [CrossRef]
15. Mandal, A.; Cui, Y.; McRae, L.; Gholipour, B. Reconfigurable chalcogenide phase change metamaterials: A material, device, and fabrication perspective. *J. Phys. Photonics* **2021**, *3*, 022005 [CrossRef]
16. Dubroka, A.; Caha, O.; Hroncek, M.; Friš, P.; Orlita, M.; Holý, V.; Steiner, H.; Bauer, G.; Springholz, G.; Humlicek, J. Interband absorption edge in the topological $Bi(Te_{1-x}Se_x)_3$. *Phys. Rev. B* **2017**, *96*, 235202. [CrossRef]
17. Siroki, G.; Lee, D.; Haynes, P. Single-electron induced surface plasmons on a topological nanoparticle. *Nat. Commun.* **2016**, *7*, 12375. [CrossRef]
18. Rider, M.S.; Sokolikova, M.; Hanham, S.M.; Navarro-Cia, M.; Haynes, P.D.; Lee, D.K.K.; Daniele, M.; Guidi, M.C.; Mattevi, C.; Lupi S.; Giannini, V. Experimental signature of a topological quantum dot. *Nanoscale* **2020**, *12*, 22817–22825. [CrossRef]
19. Kianinia, M.; Xu, Z.-Q.; Toth, M.; Aharonovich, I. Quantum emitters in 2D materials: Emitter engineering, photophysics, and integration in photonic nanostructures. *Appl. Phys. Rev.* **2022**, *9*, 011306. [CrossRef]
20. Colas des Francs, G.; Barthes, J.; Bouhelier, A.; Weeber, J.C.; Dereux, A.; Cuche, A.; Girard, C. Plasmonic Purcell factor and coupling efficiency to surface plasmons. Implications for addressing and controlling optical nanosources. *J. Opt.* **2016**, *18*, 094005. [CrossRef]
21. Chatzidakis, G.D.; Yannopapas, V. Strong electromagnetic coupling in dimers of topological-insulator nanoparticles and quantum emitters. *Phys. Rev. B* **2020**, *101*, 165410. [CrossRef]

22. Karaoulanis, D.; Paspalakis, E.; Yannopapas, V. Quantum interference near bismuth-chalcogenide microstructures. *J. Opt. Soc. Am. B* **2021**, *38*, 3301–3308. [CrossRef]
23. Kyvelos, N.; Tsigaridas, G.; Paspalakis, E.; Yannopapas, V. Quantum Interference in Spontaneous Decay of a Quantum Emitter Placed in a Dimer of Bismuth-Chalcogenide Microparticles. *Photonics* **2022**, *9*, 596. [CrossRef]
24. Vladimirova, Y.V.; Zadkov, V.N. Quantum Optics in Nanostructures. *Nanomaterials* **2021**, *11*, 1919. [CrossRef] [PubMed]
25. Agarwal, G.S. Anisotropic Vacuum-Induced Interference in Decay Channels. *Phys. Rev. Lett.* **2000**, *84*, 5500–5503. [CrossRef]
26. Paspalakis, E.; Keitel, C.H.; Knight, P.L. Fluorescence control through multiple interference mechanisms. *Phys. Rev. A* **1998**, *58*, 4868. [CrossRef]
27. Ficek, Z.; Swain, S. Simulating quantum interference in a three-level system with perpendicular transition dipole moments. *Phys. Rev. A* **2004** , *69*, 023401. [CrossRef]
28. Zhu, S.-Y.; Scully, M.O. Spectral line elimination and spontaneous emission cancellation via quantum interference. *Phys. Rev. Lett.* **1996**, *76*, 388–391. [CrossRef]
29. Menon, S.; Agarwal, G.S. Gain components in the Autler-Townes doublet from quantum interferences in decay channels. *Phys. Rev. A* **1999**, *61*, 013807. [CrossRef]
30. Evangelou, S.; Yannopapas, V.; Paspalakis, E. Simulating quantum interference in spontaneous decay near plasmonic nanostructures: Population dynamics. *Phys. Rev. A* **2011**, *83*, 055805. [CrossRef]
31. Hughes, S.; Agarwal, G.S. Anisotropy-Induced Quantum Interference and Population Trapping between Orthogonal Quantum Dot Exciton States in Semiconductor Cavity Systems. *Phys. Rev. Lett.* **2017**, *118*, 063601. [CrossRef]
32. Karanikolas, V.; Paspalakis, E. Plasmon-induced quantum interference near carbon nanostructures. *J. Phys. Chem. C* **2018**, *122*, 1478. [CrossRef]
33. Das, S.; Agarwal, G.S. Protecting bipartite entanglement by quantum interferences. *Phys. Rev. A* **2010**, *81*, 052341. [CrossRef]
34. Iliopoulos, N.; Terzis, A.F.; Yannopapas, V.; Paspalakis, E. Prolonging entanglement dynamics near periodic plasmonic nanostructures. *Phys. Rev. B* **2017**, *96*, 075405. [CrossRef]
35. Sangshekan, B.; Sahrai, M.; Asadpour, S.H. Controllable atom-photon entanglement via quantum interference near plasmonic nanostructure. *Sci. Rep.* **2022**, *12*, 677. [CrossRef]
36. Zhou, P.; Swain, S. Quantum interference in probe absorption: Narrow resonances, transparency, and gain without population inversion. *Phys. Rev. Lett.* **1997**, *78*, 832–835. [CrossRef]
37. Paspalakis, E.; Gong, S.-Q.; Knight, P.L. Spontaneous emission induced coherent effects in absorption and dispersion of a V-type three-level atom. *Opt. Commun.* **1998**, *152*, 293–298. [CrossRef]
38. Zhou, P.; Swain, S. Ultranarrow spectral lines via quantum interference. *Phys. Rev. Lett.* **1996**, *77*, 3995. [CrossRef]
39. Wang, C.-L.; Kang, Z.-H.; Tian, S.-C.; Jiang, Y.; Gao, J.-Y. Effect of spontaneously generated coherence on absorption in a V-type system: Investigation in dressed states. *Phys. Rev. A* **2009**, *79*, 043810. [CrossRef]
40. Kosionis, S.G.; Yannopapas, V.; Thanopulos, I.; Paspalakis, E. Controlling resonance fluorescence spectra and photon statistics in a driven V-Type quantum emitter—metal nanoparticle coupled structure. *Photonics* **2022**, *9*, 629. [CrossRef]
41. Evangelou, S.; Yannopapas, V.; Paspalakis, E. Transparency and slow light in a four-level quantum system near a plasmonic nanostructure. *Phys. Rev. A* **2012**, *86*, 053811. [CrossRef]
42. Evangelou, S.; Yannopapas, V.; Paspalakis, E. Modifying free-space spontaneous emission near a plasmonic nanostructure. *Phys. Rev. A* **2011**, *83*, 023819. [CrossRef]
43. Chen, H.; Ren, J.; Gu, Y.; Zhao, D.-X.; Zhang, J.; Gong, Q. Nanoscale Kerr Nonlinearity Enhancement Using Spontaneously Generated Coherence in Plasmonic Nanocavity. *Sci. Rep.* **2015**, *5*, 18315. [CrossRef] [PubMed]
44. Paspalakis, E.; Kylstra, N.J.; Knight, P.L. Transparency induced via decay interference. *Phys. Rev. Lett.* **1999**, *82*, 2079. [CrossRef]
45. Bortman-Arbiv, D.; Wilson-Gordon, A.D.; Friedmann, H. Phase control of group velocity: From subluminal to superluminal light propagation. *Phys. Rev. A* **2001**, *63*, 043818. [CrossRef]
46. Gurudev Dutt, M.V.; Cheng, J.; Li, B.; Xu, X.; Li, X.; Berman, P.R.; Steel, D.G.; Bracker, A.S.; Gammon, D.; Economou, S.E.; et al. Stimulated and spontaneous optical generation of electron spin coherence in charged GaAs quantum dots. *Phys. Rev. Lett.* **2005**, *94*, 227403. [CrossRef] [PubMed]
47. Niu, Y.-P.; Gong, S.-Q. Enhancing Kerr nonlinearity via spontaneously generated coherence. *Phys. Rev. A* **2006**, *73*, 053811. [CrossRef]
48. Asadpour, S.H.; Sahrai, M.; Soltani, A.; Hamedi, H.R. Enhanced Kerr nonlinearity via quantum interference from spontaneous emission. *Phys. Lett. A* **2012**, *376*, 147–152. [CrossRef]
49. Thanopulos, I.; Yannopapas, V.; Paspalakis, E. Non-Markovian dynamics in plasmon-induced spontaneous emission interference. *Phys. Rev. B* **2017**, *95*, 075412. [CrossRef]
50. Barnett, S.M.; Radmore, P.M. *Methods in Theoretical Quantum Optics*; Chapter 7; Oxford University Press: Oxford, UK, 1997.
51. Xu, J.-P.; Wang, L.-G.; Yang, Y.-P.; Lin, Q.; Zhu, S.-Y. Quantum interference between two orthogonal transitions of an atom in one-dimensional photonic crystals. *Opt. Lett.* **2008**, *33*, 2005. [CrossRef]
52. Yannopapas, V.; Paspalakis, E.; Vitanov, N.V. Plasmon-induced enhancement of quantum interference near metallic nanostructures. *Phys. Rev. Lett.* **2009**, *103*, 063602. [CrossRef]
53. Xu, J.-P.; Yang, Y.-P. Quantum interference of V-type three-level atom in structures made of left-handed materials and mirrors. *Phys. Rev. A* **2010**, *81*, 013816. [CrossRef]

54. Li, G.X.; Li, F.L.; Zhu, S.-Y. Quantum interference between decay channels of a three-level atom in a multilayer dielectric medium. *Phys. Rev. A* **2001**, *64*, 013819. [CrossRef]
55. Yang, Y.-P.; Xu, J.-P.; Chen, H.; Zhu, S.-Y. Quantum Interference Enhancement with Left-Handed Materials. *Phys. Rev. Lett.* **2008**, *100*, 043601. [CrossRef]
56. Li, G.-X.; Evers, J.; Keitel, C.H. Spontaneous emission interference in negative-refractive-index waveguides. *Phys. Rev. B* **2009**, *80*, 045102. [CrossRef]
57. Pelton, M. Modified spontaneous emission in nanophotonic structures. *Nat. Photon.* **2015**, *9*, 427–435. [CrossRef]
58. Yannopapas, V.; Vitanov, N.V. Spontaneous emission of two-level atoms placed within clusters of metallic nanoparticles. *J. Phys. Cond. Matter* **2007**, *19*, 096210. [CrossRef]
59. Yannopapas, V.; Vitanov, N.V. Electromagnetic Green's tensor and local density of states calculations for collections of spherical scatterers. *Phys. Rev. B* **2007**, *75*, 115124. [CrossRef]